PERGAMON

International Journal of Multiphase Flow 26 (2000) 445–466

International Journal of Multiphase Flow

www.elsevier.com/locate/ijmulflow

The effect of the dispersed to continuous-phase viscosity ratio on film drainage between interacting drops

I.B. Bazhlekov*, A.K. Chesters, F.N. van de Vosse

Centre for Polymers and Composites, Eindhoven University of Technology, P.O. Box 513, 5600 MB Eindhoven, The Netherlands

Received 18 May 1998; received in revised form 20 April 1999

Abstract

The deformation and drainage of the film between colliding drops is studied numerically at small capillary numbers, small Reynolds numbers and a range of dispersed to continuous-phase viscosity ratios, λ, covering the transition from partially-mobile to immobile interfaces. Two types of collision are considered: constant approach velocity and constant interaction force. The problem is solved numerically by means of a finite difference method for the equations in the continuous phase and a boundary integral method or finite-element method in the drops. The velocity profile in the gap between the drops is the sum of a uniform and a parabolic contribution, governed respectively by viscous forces within the dispersed and the continuous phases. Solutions to date concern the limiting cases of partially-mobile or immobile interfaces, in which either the parabolic or plug contribution is negligible. A transformation of variables then results in a universal set of governing equations. In the intermediate regime a transformed viscosity ratio, λ^*, enters these equations. In the constant-force case, the transformed drainage rate increases monotonically with λ^* and the final (rate-determining) stage of drainage is well described by a power-law dependence of the minimum film thickness on time, enabling compact analytical approximations to be developed for the drainage time. These expressions reduce to those in the partially-mobile and immobile limits for λ^*-values outside the range $10 < \lambda^* < 10^3$. In the constant-velocity case the behavior is more subtle, drainage at the periphery of the film being strongly affected by the plug contribution in the adjoining outer region. This provides an explanation for the much higher final drainage rates predicted numerically under constant-velocity conditions in the partially-mobile case. From a practical point of view the most important case to model is that dividing coalescing from non-coalescing drop collisions. While the constant-force approximation is probably closest to the final interaction in this case, the sensitivity of the drainage behavior to the outer boundary

* Corresponding author.
E-mail address: bazhleko@wfw.wtb.tue.nl (I.B. Bazhlekov).

PII: S0301-9322(99)00032-4

conditions suggests that more realistic simulations are required which take account of the actual, time-dependent interaction force/velocity.

Keywords: Drops; Coalescence; Liquid film; Drainage; Boundary integral method

1. Introduction

Drop coalescence is an essential feature of many industrial and natural processes and its prediction and control is consequently of great practical importance. The coalescence of two drops can be split conceptually into three elements (see, for example, Chesters, 1991):

1. The external flow field, governing the frequency, strength and duration of collisions.
2. The process of film formation and drainage.
3. The destabilization of the film by van der Waals and other intermolecular forces, leading to rupture.

Element (1) furnishes the initial and boundary conditions for (2), which in turn provides those for (3).

While reasonable first approximations for the collision frequency, force and duration and for the critical film-rupture thickness can be derived in many cases, film drainage is particularly sensitive to the details of the system concerned. Small tangential stresses exerted on the film by the dispersed phase or by interfacial-tension gradients translate into large forces per film volume, which strongly affect drainage rates. In pure liquid–liquid systems, exhibiting constant interfacial tension, the only tangential stresses are those exerted by the dispersed phase, arising from the internal motion within the drops generated by film drainage. The associated inertial forces are generally negligible and the retarding effect of the tangential stresses on film drainage depends on the dispersed to continuous-phase viscosity ratio, λ.

Numerical solutions of the equations governing film drainage are available in the asymptotic cases of moderate and very large λ-values, corresponding respectively to plug film flow between partially-mobile interfaces (drainage being controlled by drop viscosity) and plane Poiseuille film flow between immobile interfaces (drainage being controlled by continuous-phase viscosity). For very small λ-values, a third asymptote of fully mobile interfaces is reached, tangential stresses exerted by the dispersed phase now being negligible and drainage being controlled by viscous normal stresses in the film (continuous-phase viscosity once more controlling). The latter regime is typically encountered only for gas bubbles and is not considered further here, viscous normal stresses in the film being assumed to be negligible.

Numerical solutions for the partially-mobile limit have been obtained for both constant-force and constant-velocity interactions (Yiantsios and Davis, 1990; Saboni et al., 1995; Abid and Chesters, 1994). For the immobile limit only constant-force solutions are available (Yiantsios and Davis, 1990). Recently, Rother et al. (1997) have studied time-dependent force of interaction, based on a force balance on two spherical drops in apparent contact in buoyancy-driven flow. While first estimates suggest that the plug-flow (partial-mobility) asymptote should provide a reasonable approximation over a wide range of λ-values ($10^{-2} < \lambda < 10^{2}$: Abid and

Chesters, 1994), this range by no means covers all systems of practical interest. In addition, the range becomes narrower if very small drops are involved.

The primary objective of the present paper is to solve the governing equations over a range of λ-values spanning the transition between the two asymptotes, thereby both establishing more precisely the regime of validity of each and providing quantitative expressions for film drainage rates in the intermediate region.

In Section 2, the mathematical model is described. The model is based on a number of simplifications, in particular the restriction to gentle collisions, which have also been applied in the papers of Yiantsios and Davis (1990), Abid and Chesters (1994), Saboni et al. (1995) and Rother et al. (1997). The present study can be considered as an extension of these to unrestricted values of the dispersed to continuous phase viscosity ratio. The numerical method, tests and comparisons are presented in Section 3. In Section 4, results and discussions are presented for the cases of constant approach velocity (Section 4.1) and constant interaction force (Section 4.2). Finally, the conclusions of this study are presented in Section 5.

2. Mathematical formulation

We consider two drops of the same Newtonian fluid with viscosity μ suspended in another immiscible Newtonian fluid with viscosity μ/λ, which approach each other along the line of their centres at some specified velocity $V(t)$ (Fig. 1, t is time). Here, V is either held constant or adjusted during the drainage process to maintain a constant interaction force. The same

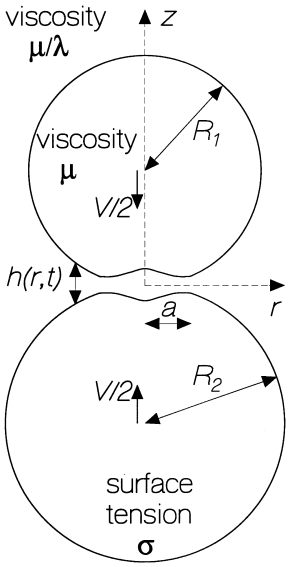

Fig. 1. Schematic sketch of the problem.

procedure can, however, be used for any function, $V(t)$, including functions more representative of actual drop collisions. The interfacial tension, σ, is supposed constant.

2.1. Approximations and simplifications

The model is based on the following approximations:

1. Small interfacial slope in the severely deformed region of the drops:

$$\frac{\partial h_i}{\partial r} \ll 1, \tag{1a}$$

where h_i ($i = 1,2$) and r denote, respectively, interfacial height and radial coordinate (Fig. 1). Eq. (1a) is satisfied if

$$a \ll R_i, \tag{1b}$$

where a (defined by Eq. (13)) denotes the radius of the film. This enables a major simplification of the governing equations, which become the same for unequal and equal drops, the equivalent equal-drop radius being given by (Chesters, 1991; Abid and Chesters, 1994)

$$R_{\mathrm{eq}}^{-1} = \frac{1}{2}\left(R_1^{-1} + R_2^{-1}\right) \tag{2}$$

In addition, the interface may be approximated as plane as far as flow in the drop is concerned. As noted by Chesters (1991), Eq. (1b) is not as restrictive as it appears since only for gentle collisions drainage is typically rapid enough for coalescence to occur.
2. The considerations are limited to the viscous regime, in which the inertial forces in the film and the adjacent dispersed-phase flow are negligible.
3. The influence of viscous normal stresses in the film is neglected, allowing the quasi-parallel flow in the film to be approximated as the sum of a plug (uniform) and parabolic profile.
4. The influence on film drainage of viscous normal stresses and pressure variation in the drop is neglected.
5. The effects of body forces or acceleration of the reference frame are neglected.

The regime of validity of these approximations has been discussed by Abid and Chesters (1994).

2.2. Governing equations

Taking Eq. (1) into account, the continuity and Navier–Stokes equations in the film can be expressed in integral form:

$$\frac{\partial h}{\partial t} = -\frac{1}{r}\frac{\partial (rhu)}{\partial r}, \tag{3}$$

$$\tau = -\frac{h}{2}\frac{\partial p}{\partial r}, \tag{4}$$

where $h = h_1 - h_2$ is the gap thickness, τ the tangential stress exerted on the interface by the film, p the pressure in the film and u the mean velocity in the film, consisting of the sum of uniform and parabolic parts, u_u and u_p, respectively:

$$u = u_u + u_p = u_u - \frac{\lambda}{12\mu}h^2\frac{\partial p}{\partial r}, \tag{5}$$

Note that u_u is also the interface velocity. In general both parts, being of order $O(h^2)$ and $O(h^3)$ respectively ($\partial p/\partial r \sim O(h)$), could be important for the flow in the gap:

- the parabolic part outside the film region $r \gg a$ (relatively large h) even at small values of λ;
- the uniform part in the film region $r < a$ at the last stage of drainage ($h \ll a$) even for large λ.

Within the drops, the continuity and Navier–Stokes equations are:

$$\nabla \cdot v = 0 \tag{6}$$

$$-\nabla p_d + \mu\nabla^2 v = 0, \tag{7}$$

where p_d is the pressure and v the velocity in the drop.

The boundary conditions at the interfaces consist of continuity of tangential velocity and stress, together with a jump in normal stress (i.e. pressure) associated with the interfacial tension:

$$u_u = v_r \tag{8}$$

$$\tau = \tau_d \tag{9}$$

$$p = \frac{2\sigma}{R_{eq}} - \frac{\sigma}{2}\left(\frac{\partial^2 h}{\partial r^2} + \frac{1}{r}\frac{\partial h}{\partial r}\right) \tag{10}$$

where use has be made of Eqs. (1) and (2). The outer boundary conditions at sufficiently large r, r_{large}, are:

$$p(r_{large}) = 0 \tag{11}$$

and either

$$\left(\frac{\partial h}{\partial t}\right)_{r_{large}} = -V(t) \tag{12}$$

or

$$2\pi \int_0^{r_{\text{large}}} pr \, \mathrm{d}r = F(t) = \frac{2\pi (a(t))^2 \sigma}{R_{\text{eq}}} \tag{13}$$

In the constant-velocity and constant-force cases investigated in the present paper, V and F are, respectively, the drop approach velocity and interaction force and they are considered to be constant with respect to the time; a is a measure of the film radius (a = constant, in the constant-force case).

The initial condition is

$$h = h_0 + \frac{r^2}{R_{\text{eq}}}, \quad t = 0 \tag{14}$$

which corresponds to undeformed drops ($p = 0$ in Eq. (10)).

2.3. Transformed dimensionless equations

A transformation of the variables in Eqs. (3)–(14) is possible, which renders them dimensionless and reduces the number of parameters to one: a dimensionless group containing the viscosity ratio λ. The required transformation is different in the constant-velocity and constant-force cases, for details see Chesters (1991), Abid and Chesters (1994) and Saboni et al. (1995).

Constant approach velocity:

$$r^* = \frac{r}{Ca^{1/3} R_{\text{eq}}}; \quad h^* = \frac{h}{Ca^{2/3} R_{\text{eq}}}; \quad t^* = \frac{tV}{Ca^{2/3} R_{\text{eq}}}; \quad \tau^* = \tau_{\text{d}}^* = \frac{\tau Ca^{2/3} R_{\text{eq}}}{\mu V}; \quad z^* = \frac{z}{Ca^{1/3} R_{\text{eq}}};$$

$$p^* = \frac{p R_{\text{eq}} Ca}{\mu V}; \quad p_{\text{d}}^* = \frac{p_{\text{d}} R_{\text{eq}} Ca^{2/3}}{\mu V}; \quad u^* = \frac{u Ca^{1/3}}{V}; \quad v^* = \frac{v Ca^{1/3}}{V}; \quad \lambda^* = \lambda Ca^{1/3}$$

where Ca is the capillary number, $Ca = \mu V/\sigma$.

Constant interaction-force:

$$r^* = \frac{r}{R_{\text{eq}} a'}; \quad h^* = \frac{h}{R_{\text{eq}} a'^2}; \quad t^* = \frac{t\sigma a'}{R_{\text{eq}} \mu}; \quad \tau^* = \tau_{\text{d}}^* = \frac{\tau \, R_{\text{eq}}}{\sigma a'}; \quad z^* = \frac{z}{R_{\text{eq}} a'};$$

$$p^* = \frac{p R_{\text{eq}}}{\sigma}; \quad p_{\text{d}}^* = p_{\text{d}} \frac{R_{\text{eq}}}{\sigma a'}; \quad u^* = \frac{\mu \mu}{\sigma a'^2}; \quad v^* = \frac{v\mu}{\sigma a'^2}; \quad \lambda^* = \lambda a'$$

where a' is the dimensionless radius of the film: $a' = a/R_{\text{eq}}$.

Remark. *The dispersed-phase variables z and p_{d} are seen to transform differently from their continuous-phase counterparts h and p. This in fact justifies the approximations (1) and (4). For example, since $z_{\text{interface}} = h/2$,*

$$\frac{\partial z_{\text{interface}}}{\partial r} = \frac{1}{2}\frac{\partial h}{\partial r} \text{ yielding } \frac{\partial z^*_{\text{interface}}}{\partial r^*} \to \frac{\alpha}{2}\frac{\partial h^*}{\partial r^*},$$

where α stands for $Ca^{1/3}$ or a'. In the small-α limit, therefore, a significant value of $\partial h^*/\partial r^*$ translates into a negligible value of $\partial z^*_{\text{interface}}/\partial r^*$, justifying treatment of the interface as plane in transformed coordinates as far as the drop flow is concerned.

Applying the above transformations to Eqs. (3)–(14) a set of dimensionless governing equations is obtained, containing only one parameter, λ^*. Two additional parameters, h_0^* and r^*_{large} enter the problem via the initial and boundary conditions, but these prove of no influence provided chosen sufficiently large.

The governing Eqs. (3)–(14) in transformed variables take the form:

- Equations in the film, see Eqs. (3)–(5):

$$\frac{\partial h^*}{\partial t^*} = -\frac{1}{r^*}\frac{\partial\left(r^* h^* u^*_{\text{u}}\right)}{\partial r^*} + \frac{1}{r^*}\frac{\lambda^*}{12}\frac{\partial}{\partial r^*}\left(h^{*3} r^* \frac{\partial p^*}{\partial r^*}\right) \tag{15}$$

$$\tau^* = -\frac{h^*}{2}\frac{\partial p^*}{\partial r^*}, \tag{16}$$

- equations in the drops, see Eqs. (6) and (7):

$$\nabla^* \cdot v^* = 0 \tag{17}$$

$$-\nabla^* p^*_{\text{d}} + \nabla^{*2} v^* = 0 \tag{18}$$

- boundary conditions at the interfaces, see Eqs. (8)–(10):

$$u^*_{\text{u}} = v^*_r \tag{19}$$

$$\tau^* = \tau^*_{\text{d}} \tag{20}$$

$$p^* = 2 - \frac{1}{2}\left(\frac{\partial^2 h^*}{\partial r^{*2}} + \frac{1}{r^*}\frac{\partial h^*}{\partial r^*}\right) \tag{21}$$

- initial condition, see Eq. (14):

$$h^*(r^*, t^* = 0) = h_0^* + r^{*2} \tag{22}$$

- outer boundary conditions, see Eqs. (11)–(13):

$$p^*\left(r^*_{\text{large}}\right) = 0 \tag{23}$$

$$-\left(\frac{\partial h^*}{\partial t^*}\right)_{r^*_{\text{large}}} = V^* = 1 \tag{24}$$

in the constant-velocity case or

$$\int_0^{r^*_{\text{large}}} p^* r^* \, \mathrm{d}r^* = 1 \tag{25}$$

in the constant-force case.

3. Numerical method

3.1. Numerical scheme

The solution scheme for the constant-velocity case (Eqs. (15)–(24)) is as follows. Starting from a given $h^*(r^*)$, given by Eq. (22), p^* is calculated from Eq. (21) and τ^* from Eq. (16), providing (via Eq. (20)) the boundary condition for Eqs. (17) and (18). The solution of these equations in the drops then furnishes u^*_{u} via Eq. (19). Now having u^*_{u} and p^* the film thickness at the next time instant can be obtained from Eq. (15) and the whole process is repeated.

Eqs. (17) and (18), governing the flow in the drop, are solved using one of the following methods, approximating the interface as flat:

The boundary integral method (BIM), providing a direct relation between u^*_{u} and τ^* (Davis et al., 1989):

$$u^*_{\mathrm{u}}(r^*) = \int_0^{r^*_{\text{large}}} \phi\left(r^*, r'\right) \tau^*(r') \, \mathrm{d}r', \tag{26}$$

where the elliptic Green's function kernel $\phi(r^*, r')$ is

$$\phi\left(r^*, r'\right) = \frac{r'}{4\pi} \int_0^{2\pi} \frac{\cos\theta \, \mathrm{d}\theta}{\left(r^{*2} + r'^{\,2} - 2r^* r' \cos\theta\right)^{1/2}} \tag{27}$$

Special attention is paid to the singularity of Eq. (27), which appears at $r^* = r'$.

A finite element method (FEM), which has the advantage of providing information on the flow in the drops and can be extended to a more general constitutive equation (e.g. general viscous or viscoelastic dispersed phase), but the disadvantage that it may consume more CPU time. As the results obtained by both methods are the same, in most of the cases BIM is used here. The FEM is used only when we need information about the flow in the drops.

Eq. (15) is a nonlinear, fourth-order, hyperbolic-type partial differential equation with respect to h^*. An Euler explicit scheme of first order with respect to t^* is used for the time derivative and a finite difference scheme of second order on non-uniform mesh for the spatial derivatives. Because this equation is very stiff as has been mentioned by Rother et al., especially for high λ^*, special attention must be paid to it. It can be shown that the requirements for numerical stability of Eq. (15) arising from the plug and parabolic parts of the flow (the first and second terms on the rhs of Eq. (15)) are respectively:

$$(\Delta t^*)_I \leq \text{const} \cdot \min_{j=0,n} \left(\frac{\Delta r_j^{*3}}{h_j^{*2}} \right), \tag{28a}$$

and

$$(\Delta t^*)_{II} \leq \frac{24}{\lambda^*} \min_{j=0,n} \left(\frac{\Delta r_j^{*4}}{h_j^{*3}} \right), \tag{28b}$$

where j are the numbers of the nodes r_j^* in the mesh, Δt^* is the time step, $\Delta r_j^* = r_j^* - r_{j-1}^*$ are the space steps, and h_j^* are the values of h^* in the nodes r_j^*. Eq. (28b) is much more restrictive than Eq. (28a), especially for large λ^*. However, the computation of the second term on the rhs of Eq. (15) consumes much less CPU time than the first, plug term, which depends via u_u^* on the solution of Eqs. (17) and (18). Based on these features a multiple time step approach has been developed (see Bazhlekov and van de Vosse, 1998) with automatic choice of the time steps, $(\Delta t^*)_I$ and $(\Delta t^*)_{II}$, according to Eq. (28).

To avoid very small time steps (time steps used in the present calculations are in the interval 10^{-4}–10^{-9}) non-uniform meshes are generated accordingly to the values of h_j^*, very small constant step, Δr_f^*, in the film region, $0 < r^* < 1.3$, where the most severe deformation appears; increasing by a geometrical-progression law at large r^*, becoming of order 0.5 at the end of the computational domain ($r^* = r_{\text{large}}^*$). Choosing the parameter of the geometrical progression (ratio between two following steps) very close to 1 the generated meshes locally are almost uniform. The coarse part of the mesh $\Delta r^* \sim O(1)$ far from the film region does not introduce additional errors, because the interfaces differ only slightly from a parabola and the second-order accuracy scheme, which is used, is exact for parabolas. In most of the constant-force calculations three different meshes are used:

- $\Delta r_f^* \sim 0.05$ at the beginning, prior to significant deformation ($h_{\min}^* > 1$);
- $\Delta r_f^* \sim 0.02$ during the film formation ($0.1 < h_{\min}^* < 1$);
- $\Delta r_f^* \sim 0.01$ after the dimple is formed.

In the case of constant approach velocity the same approach is used, however the finest part of the mesh is progressively extended following the expansion of the dimple. Thus, the number of the nodes in the last stage of drainage is of order 150–300 of which more than 2/3 are located in the dimple region.

To avoid any perturbations arising from remeshing, a spline interpolation is used to calculate h_j^* in the nodes of the new mesh.

The value of r_{large}^* is chosen such that $\tau^*(r_{\text{large}}^*) \ll 1$, so that the error introduced in the integration of Eq. (26) by truncating the interface is small enough. Thus, in the constant-velocity case $r_{\text{large}} = 30$ and in constant-force one $r_{\text{large}}^* = 10$ (at $\lambda^* = 0$; $r_{\text{large}}^* = 20$). The value of h_0^* is chosen to be 2 in the constant-velocity case, which is the value used in the previous paper by Abid and Chesters (1994) and 8 in constant-force one.

In the constant-force case, because of the initial condition (22) for which $p^* = 0$ and the explicit numerical scheme used, Eq. (25) is not satisfied initially. Thus, the imposed approach velocity (given by the rhs of Eq. (24)) is held constant at some initial value, V_{appr}^*, until Eq. (25) is satisfied. This velocity is then decreased, finally becoming almost zero, in such a way as

to continually satisfy Eq. (25). For the results presented in the next section, Eq. (25) is satisfied within an error of less than 0.1%.

The implicit numerical scheme used by Yiantsios and Davis and improved recently by Rother et al. is more efficient with respect to the CPU time than that used here. However, in the present approach the film equation (15) and drop Eqs. (17) and (18) are solved independently and the method can therefore be extended to simulations involving nonlinear dispersed-phase equations, arising from heat-mass transfer or non-Newtonian viscous or viscoelastic constitutive equations. In contrast, the approach used by Rother et al. (1997) is restricted to drop flow governed by linear equations only (their linear matrix relation (4.8) between the tangential stress and velocity).

3.2. Numerical tests

In order to check the sensitivity of the solution to the values of the extra parameters of the mathematical model (r^*_{large}, h^*_0, the spatial resolution and V^*_{appr} in the constant force case) and to optimize these values, a number of tests have been performed. In Fig. 2 results for $h^*_{\min}(t^*)$ in the case of constant interaction force at $\lambda^* = 100$ are shown for different values of the extra parameters. The solid line corresponds to the reference values, $r^*_{\text{large}} = 10$; $h^*_0 = 8$; $V^*_{\text{appr}} = 20\lambda^* = 2000$, and is obtained using 190 mesh nodes with resolution $\Delta r^*_{\text{f}} = 0.01$. These reference values have been used in most of the constant-force calculations (with the exception of $\lambda^* = 0$, for which $r^*_{\text{large}} = 20$). Fig. 2 indicates that further increase in the values of the parameters or spatial resolution has a negligible influence on the film drainage (for

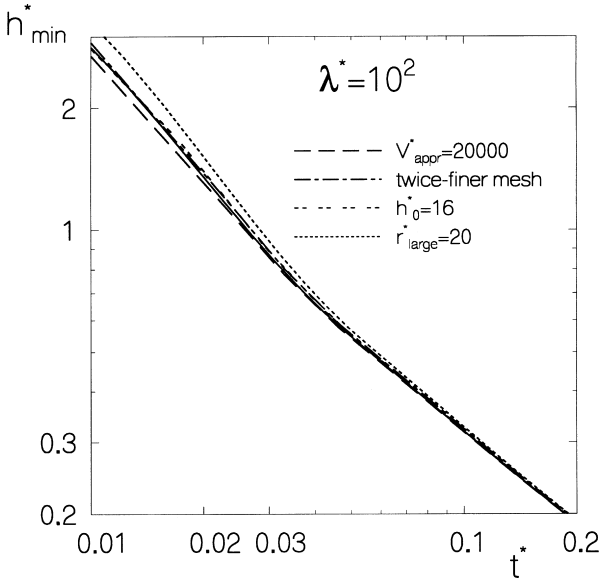

Fig. 2. The influence of the extra parameters, V^*_{appr}, h^*_0, r^*_{large} and the number of the nodes in the mesh on the results at $\lambda^* = 10^2$ (constant interaction force, $\lambda^* = \lambda a'$). Thick line corresponds to the reference values of these parameters, $V^*_{\text{appr}} = 20\lambda^* = 2000$, $h^*_0 = 8$, $r^*_{\text{large}} = 10$ and number of the nodes, 190 ($\Delta r^* = 0.01$ for $r^* < 1.3$).

$h^*_{\min}(t^*) < 0.3$). The time steps restricted by the numerical stability conditions (28) are already small enough and their further decrease does not change the results at all.

3.3. Comparisons with previous numerical results

In order to check the ability of the presented numerical approach to solve the mathematical model Eqs. (3)–(14) a number of comparisons with the available numerical and analytical results in the partially-mobile and immobile limits have been performed ($\lambda^* = 0$ and ∞, respectively). Comparisons with the numerical results of Abid and Chesters (1994) and asymptotic results of Yiantsios and Davis (1990) are presented in Sections 4.1 and 4.2, respectively.

In the present section comparisons with Saboni et al. and Rother et al. in the partially-mobile limit for constant interaction force are discussed. Saboni et al. have presented numerical results of the evolution of the film thickness profiles (their figure 2). However, they have predicted a value of the dimple radius about $r^*_D = 1.2$ in contrast with previous as well as present study (see Fig. 9a) which indicates that r^*_D is very close to unity. Rother at al. have discussed this discrepancy and concluded that the main reason is the inability of the explicit method used by Saboni et al. or its modification to yield accurate results for film-drainage model concerned. We think, however, that the main reason for the mentioned discrepancy is that Saboni et al. did not satisfy the constant-force boundary condition (their equation 15) early enough in the drainage process: their figure 3 suggests that this condition is only satisfied at the largest t^*-value ($t^* = 50$).

In order to check the validity of the explicit numerical scheme described in the present

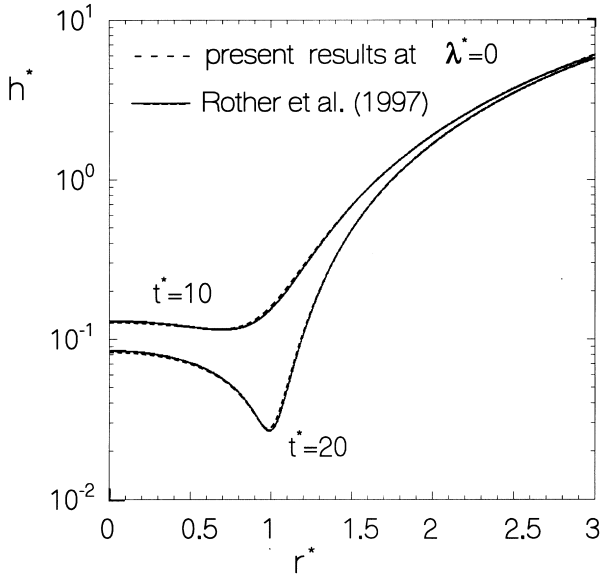

Fig. 3. Comparison between the present numerical results (dashed lines) and these of Rother et al. (thick lines) with respect to the film thickness profile at $\lambda^* = 0$ and $A^* = 10^{-4}$ (constant interaction force).

section, comparisons with the results of Rother et al., who used a fully implicit numerical technique, have been performed. For this purpose the intermolecular van der Waals attraction forces have been included in the model. (An extensive investigation of the overall influence of the viscosity ratio and intermolecular forces will appear in a separate paper). In the partially-mobile case ($\lambda^* = 0$) this affects only Eq. (16) which becomes (see Saboni et al. (1995) and Rother et al. (1997)):

$$\tau^* = -\frac{h^*}{2}\frac{\partial p^*}{\partial r^*} + \frac{A^*}{h^{*3}}\frac{\partial h^*}{\partial r^*} \tag{29}$$

where $A^* = A/(4\pi\sigma R_{eq}^2 a'^6)$ and A is the Hamaker constant. This change of the mathematical model does not necessitate any changes in the numerical algorithm. Only the mesh is refined at the periphery of the dimple, where the spatial steps are of order of magnitude smaller ($\Delta r^* = 0.001$) in order to approximate the extremely high gradients of τ^*, p^* and u^* accurately.

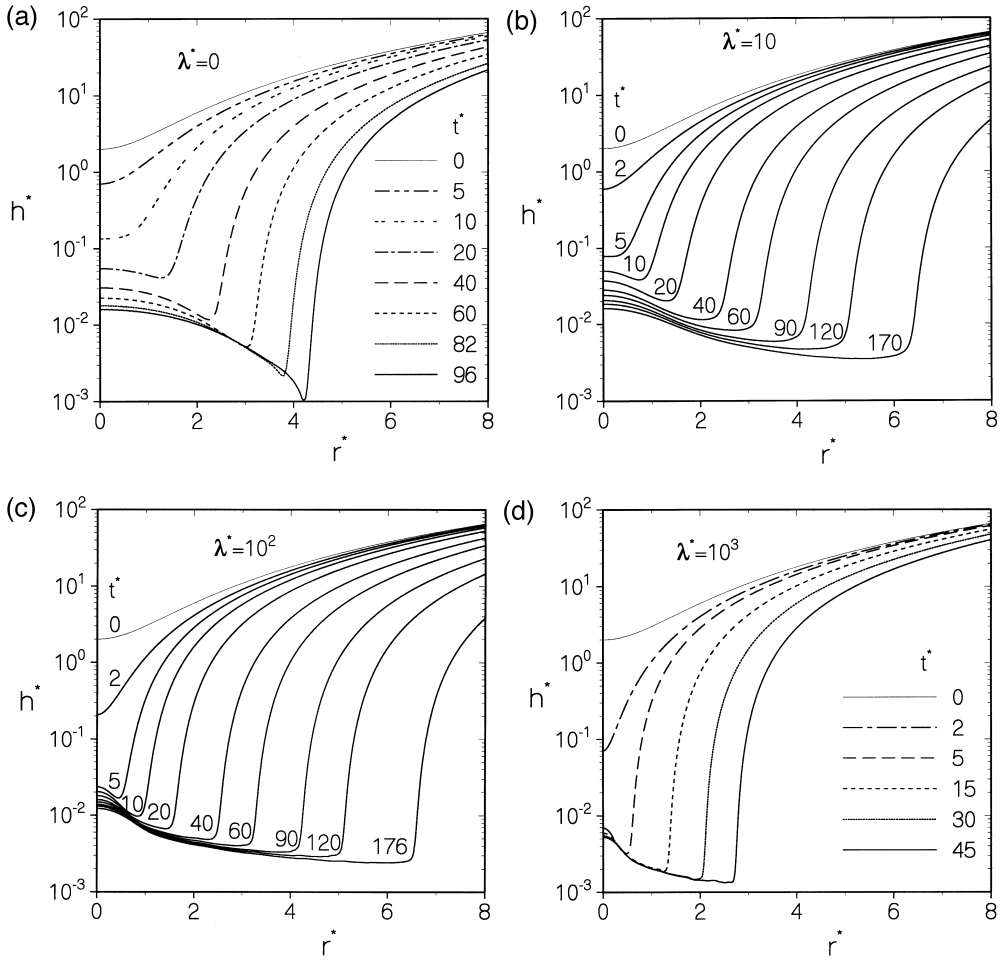

Fig. 4. Time evolution of the film thickness for different λ^* values (constant approach velocity, $\lambda^* = \lambda Ca^{1/3}$).

In Fig. 3 a comparison between the present results (dashed lines) and Rother et al.'s (thick lines) for $\lambda^* = 0$ and $A^* = 10^{-4}$ are shown. The only differences between the two simulations are:

- the numerical approach (purely explicit in the present case and fully implicit in the approach used by Rother et al.);
- a different initial separation, $h_0^* = 8$ (dashed lines) and $h_0^* = 4$ (thick lines), which results in a difference with respect to t^* of about 1.8 (the time, t^*, of the present results is translated with -1.8).

The comparisons with respect to the rupture time at different A^*-values are also in good agreement with Rother et al.'s (their figure 5).

Based on the above comparisons it can be concluded that the present explicit numerical scheme can be a successful alternative to the available implicit ones, especially for simulation of film drainage in coalescing non-Newtonian dispersions.

4. Results and discussion

4.1. Constant approach velocity

For all results presented in this case $h_0^* = 2$ and $r_{\text{large}}^* = 30$. Fig. 4 displays the variation of the transformed film thickness $h^*(r^*)$ with time for four values of λ^*. The results for $\lambda^* = 0$ (Fig. 4a) agree well with those obtained by Abid and Chesters (1994) except at very large times ($t^* > 50$), for which the present computations predict higher drainage rates (Fig. 5). The present results are seemed to be more reliable in view of the procedure of grid refinement adopted. Abid and Chesters already found final values of $-\mathrm{d}h_{\min}/\mathrm{d}t$ to be higher than those in

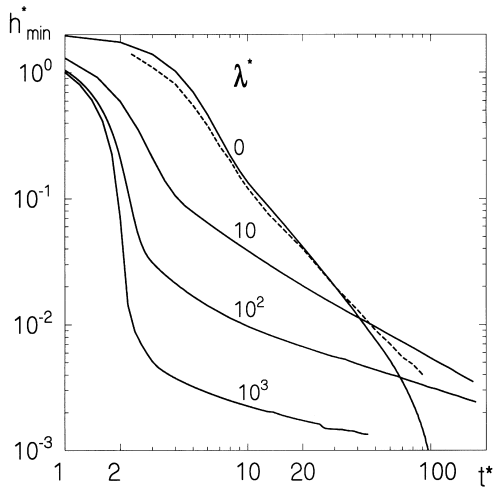

Fig. 5. Variation of the minimal film thickness as a function of the time for different λ^* (constant approach velocity). Present results (thick lines); Abid and Chesters' results for $\lambda^* = 0$ (dashed line).

the constant-force case (for given values of a and $h_{\min}$) and this result is thus strengthened further. This difference between the constant-velocity and constant-force cases must arise from the difference in outer boundary conditions, the imposed approach velocity, V, being constant in one case and falling towards zero in the other. The mechanism by which $V(t)$ affects the final stages of drainage emerges from the results obtained for non-zero λ^*-values, as discussed below. The flow pattern within the drop, obtained by FEM simulation, is shown in Fig. 6.

The influence of λ^* on the development of the film and on the transformed drainage rate, $-\mathrm{d}h^*_{\min}/\mathrm{d}t^*$, is seen from Fig. 4 and Fig. 5, respectively. Keeping in mind that the transformations for h^*, r^* and t^* involve only the dispersed-phase viscosity, the progression from Fig. 4a to Fig. 4d may be viewed as the effect of reducing the continuous-phase viscosity, starting from a value for which the parabolic contribution to film flow is negligible. Intuitively, this would be expected to provoke a monotonic increase in the drainage rate. Fig. 5 indicates, however, that while this increase is observable initially, at large t^*-values drainage is fastest for $\lambda^* = 0$. Additionally, for $\lambda^* = 0$ the dimple becomes much more pronounced.

To understand this result the ratio between the parabolic and plug contributions was examined. Fig. 7 shows the result for $\lambda^* = 10$. Except in the early stages of drainage, the parabolic contribution is negligible within the film, though dominant just outside it. If the

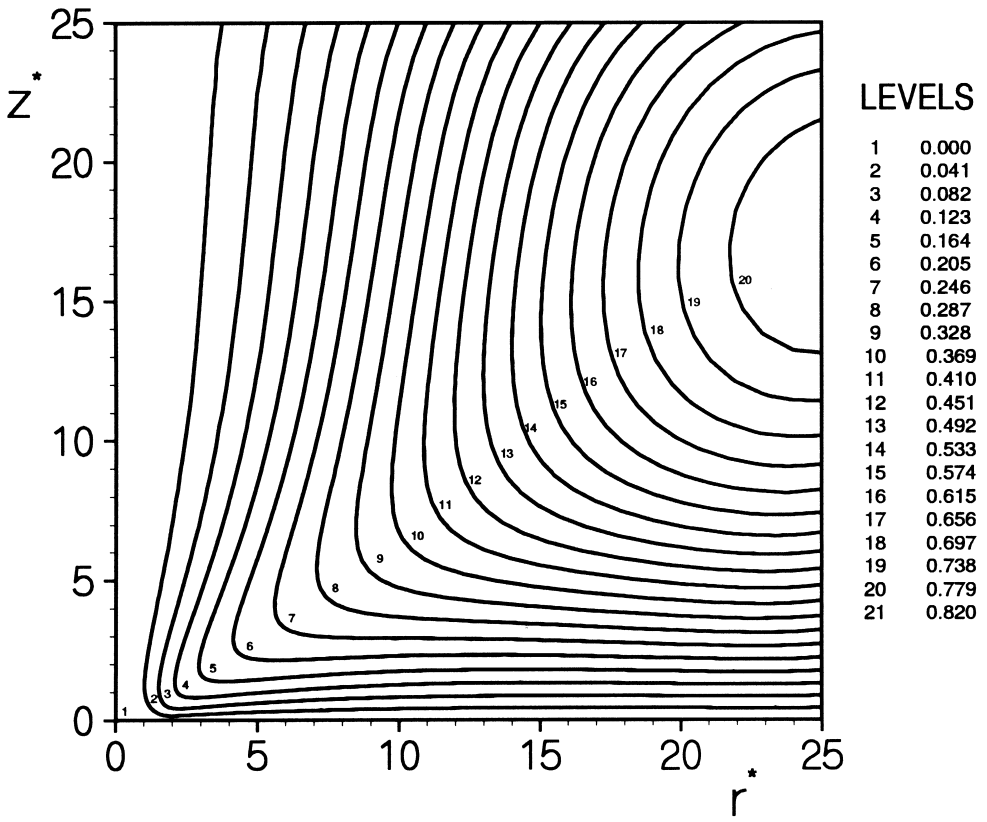

Fig. 6. Flow pattern within the drop for $\lambda^* = 10$ and $t^* = 20$ (constant approach velocity).

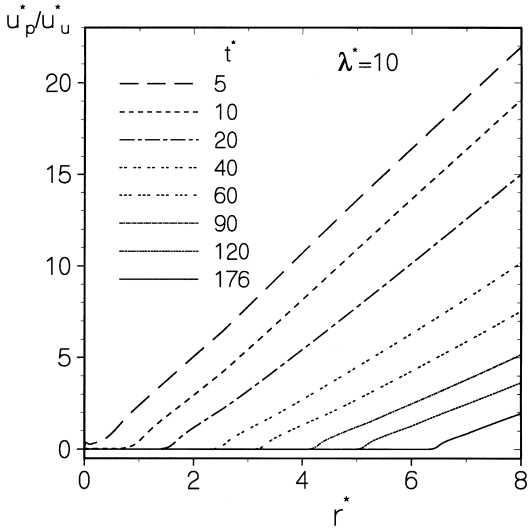

Fig. 7. Variation of the ratio between the parabolic and uniform contributions to the mean velocity in the film for $\lambda^* = 10$ (constant approach velocity).

influence of this outer region is small the later stages of drainage should therefore closely resemble those for $\lambda^* = 0$, aside from any history effects arising from the greater role of the parabolic contribution in the early stages of drainage. An alternative possibility is that the flow in the outer region drives the drop circulation, thereby strongly affecting the thinning rate at the edge of the film.

To choose between these possibilities the following numerical experiment was performed: the film shape for $\lambda^* = 10$, $t^* = 120$ was taken as initial condition for a computation using $\lambda^* = 0$.

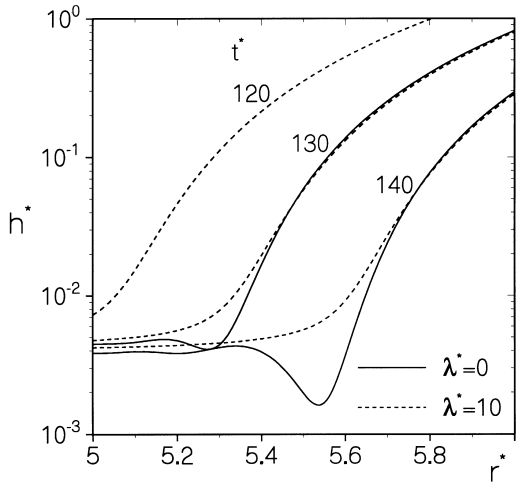

Fig. 8. Evolution of the film thickness with time for $\lambda^* = 10$ (dashed lines) and $\lambda^* = 0$ (thick lines), taking the results for $\lambda^* = 10$ and $t^* = 120$ as initial condition (constant approach velocity).

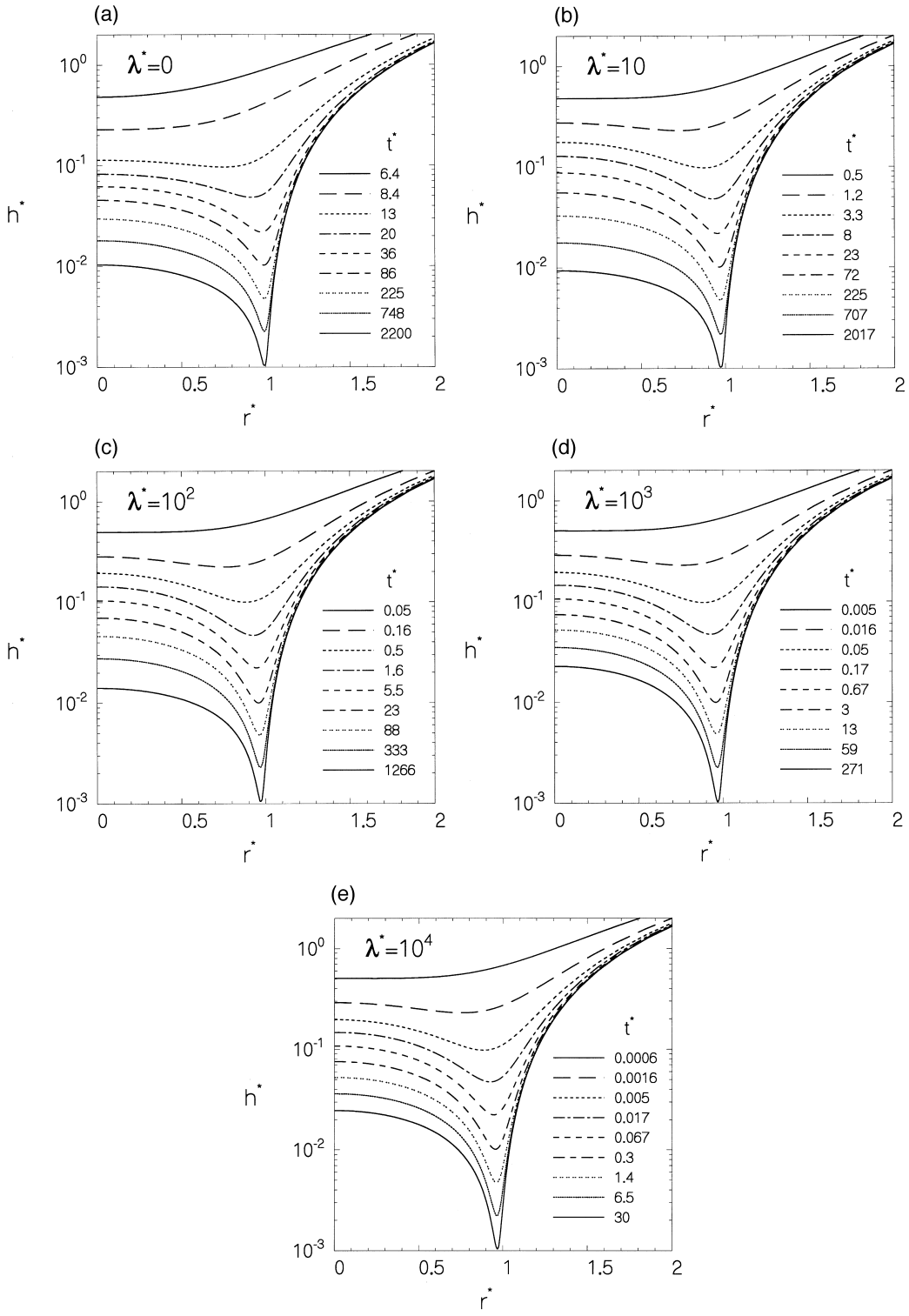

Fig. 9. Time evolution of the film thickness for different values of λ^* (constant interaction force, $\lambda^* = \lambda a'$).

If history effects are primarily responsible for the observed influence of λ^*, the ensuing drainage should now closely resemble that for $\lambda^* = 10$. The results of this experiment are shown in Fig. 8. It is seen that the elimination of the parabolic contribution for $t^* > 120$ dramatically accelerates drainage at the periphery of the film, which becomes more like that in Fig. 4a. This shows that the parabolic contribution to the flow, though negligible in the thinnest region of the film, nevertheless strongly influences drainage there. The effect presumably results from the strong influence of the parabolic contribution on interfacial velocities in the outer region. In this region the interfaces are only slightly deformed and the mean velocity, u^*, is virtually independent of λ^*, being determined by continuity. For $\lambda^* = 10$, much the greater contribution to u^* arises from the parabolic contribution, u_p^*, and the interfacial velocity, u_u^*, is consequently small ($u_u^* \ll u^*$), whereas for $\lambda^* = 0$, $u_u^* = u^*$. The more higher interfacial velocity in the outer region when $\lambda^* = 0$ is communicated via viscous action within the drop to the inner region, leading to more pronounced dimple development and greatly accelerated drainage at the periphery of the film.

A further check on the preceding explanation is provided by the influence of λ^* in the constant-force case. In this case, the approach rate of the interfaces in the region outside the film is extremely small in the final stages of drainage. Even for $\lambda^* = 0$ therefore, interfacial velocities in the outer region are small and the presence of a parabolic component should have little effect. This indeed proves to be the case (Section 4.2).

4.2. Constant interaction force

In the constant-force case a number of numerical tests indicate (see Section 3.2) that the initial, constant-velocity phase of drainage is without influence on the final behavior provided Eq. (25) is satisfied well before the formation of the dimple. For the results presented in the present section Eq. (25) is satisfied at $h_{min}^* > 7.5$, while the film is formed at $h_{min}^* < 1$. The

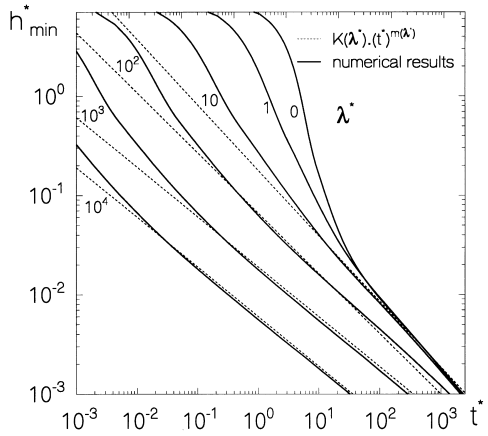

Fig. 10. Variation of the minimal film thickness as a function of the time for different λ^* (constant interaction force), numerical results (thick lines) and asymptotic formulae (30),(33), for $\lambda^* \geq 10$ (dashed lines).

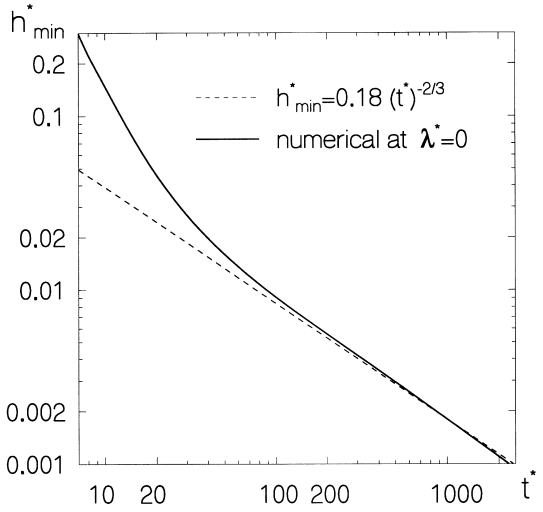

Fig. 11. Comparison between the present numerical results for $\lambda^* = 0$ (thick line) and Eq. (31) (dashed line).

required initial approach velocity, V^*_{appr}, increases with λ^* and at $h^*_0 = 8$ it is $V^*_{\text{appr}} = 5$ for $\lambda^* = 0$ and $V^*_{\text{appr}} = 20\lambda^*$ for $\lambda^* \geq 1$.

In Figs. 9 and 10 the time evolution of h^* and $h^*_{\min}$ is shown for different values of λ^*. It is seen from Fig. 9a–e that with increasing λ^* the dimple, is formed at larger $h^*_{\min}$ and the depth of the dimple $(h^*(0) - h^*_{\min})$ in the later stages of drainage also increases. The only exception is the approach to partial mobility, $\lambda^* \leq 10$, for which the dimple depth decreases with increasing λ^*. As discussed in Section 4.1, this behavior at small λ^*-values results from the influence of the outer region flow via the flow in the drop. An accompanying effect is a small change in the value of the final dimple radius, r^*_{D}, from 0.99 for $\lambda^* = 0$ to 0.97 for $\lambda^* \geq 10$. More detailed investigation shows that the final dimple radius is 0.97 even for very small $\lambda^* = 0.01$. This deviation from the value for $\lambda^* = 0$ again results from the influence of the parabolic part of the film flow in the outer region

The case $\lambda^* = 0$ has been examined by Yiantsios and Davis (1990). The results of Yiantsios and Davis are seen to agree well with the present ones when expressed in terms of the transformed variables (Fig. 11).

Fig. 10 indicates that the drainage rate increases monotonically with λ^*, in contrast with the constant-velocity case. Once the dimple becomes pronounced[1] the drainage rate is well approximated for all λ^*-values by a simple power law:

$$h^*_{\min} = \frac{K(\lambda^*)}{(t^*)^{m(\lambda^*)}} \tag{30}$$

Eq. (30) is consistent with Yiantsios and Davis' results in the small and large-λ^* limits (their

[1] Typically when $h^*_{\min} < 0.1$. However, for $\lambda^* = 0$, Eq. (30) becomes a good approximation somewhat later: $h^*_{\min} < 0.03$ (see also Fig. 11).

equations (70) and (37) respectively) which, when expressed in the present transformed variables, become (see Appendix A)

$$h^*_{\min} = \frac{0.18}{(t^*)^{2/3}}, \qquad \lambda^* \to 0 \tag{31}$$

$$h^*_{\min} = \frac{0.6}{(\lambda^* t^*)^{1/2}}, \qquad \lambda^* \to \infty \tag{32}$$

As noted earlier, the small-λ^* limit Eq. (31) agrees well with the present results (see Fig. 11). Fig. 10 indicates that it also provides a good approximation for λ^*-values up to 10 provided $h^*_{\min}$ is small enough ($h^*_{\min} \leq 0.03$). For larger $h^*_{\min}$-values, however, the range of λ^* -values for which the approximation of partial mobility applies is narrower.

The large-λ^* limit Eq. (32) becomes a reasonable approximation if $\lambda^* \geq 10^3$ (Fig. 12). Since the present considerations are based on the restriction $a' \ll 1$ (Eq. (1b)), the approximation of partial interfacial mobility will typically be a good one up to λ-values of at least 10^2 while the approximation of interfacial immobility will be a good one only if λ is at least 10^4. This statement pre-supposes that dimpling precedes rupture. For very small drops this may not be the case and the upper λ-limit at which the approximation of partial mobility fails will then be smaller.

From a practical point of view it is useful to derive analytical, albeit approximate, expressions for $m(\lambda^*)$ and $K(\lambda^*)$ in the range of λ^*-values for which neither Eqs. (31) nor (32) are satisfactory ($10 < \lambda^* < 10^3$). Fig. 10 shows that a reasonably good fit of the numerical results over all λ^*-values is provided by the empirical expressions

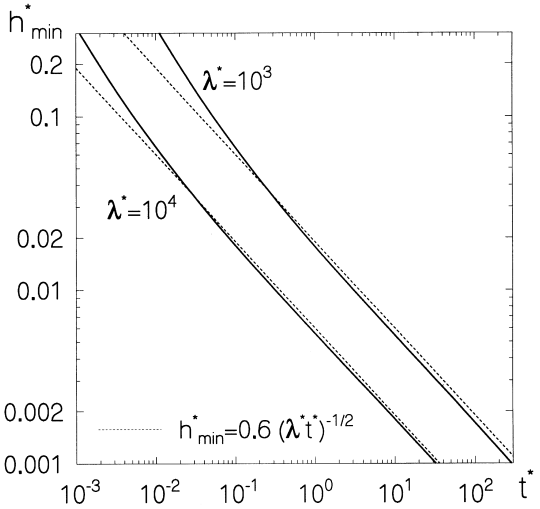

Fig. 12. Comparison between the numerical results for $\lambda^* = 10^3$ and 10^4 (thick lines) and Eq. (32) (dashed lines).

$$m(\lambda^*) = \frac{1}{2} + \frac{(1/6)}{1.0045^{\lambda^*}}, \qquad K(\lambda^*) = \frac{0.18}{(0.09\lambda^*)^{0.5(1-1.025^{-\lambda^*})}} \tag{33}$$

Eq. (33) reduces to the values of m and K given by Eqs. (31) and (32) in the small and large-λ^* limits.

Yiantsios and Davis also proposed a power-law relation like Eq. (30) for the thickness at the film centre in the small and large-λ^* limits. Such a relation does not, however, adequately describe the results obtained in the intermediate range of λ^*-values, except perhaps at such large values of t^* that $h^*_{\min}$ would in reality have long since attained the critical rupture thickness.

5. Conclusions

The present results bridge the gap between existing film-drainage models for partially-mobile and immobile interfaces under constant-force or constant-velocity conditions. In the constant-force case, the final (rate-determining) phase of drainage proves to be well described by a power-law dependence of the minimum film thickness on time, enabling compact analytical approximations to be developed for the drainage time (Eqs. (30) and (33)). These expressions reduce to those in the partially-mobile and immobile limits for λ^*-values outside the range $10 < \lambda^* < 10^3$.

The results also shed light on the influence of the collision boundary conditions (constant-force versus constant-velocity) on the final phase of drainage. Any outward interfacial motion in the region just beyond the film communicating via viscous action to the film itself, thereby strongly increasing the thinning rate at the edge of the film.

With the exception of gravity-driven drainage between a drop and a free interface, real collisions are characterized neither by a constant interaction force nor by a constant approach velocity. Typically the interaction force rises to a maximum as the approach velocity falls to zero, after which the drops begin to separate again if coalescence has not occurred. From a modelling point of view, the situation of greatest importance is that dividing coalescing from non-coalescing collisions, in which the required drainage time is just equal to that available. The final stages of drainage then take place around the point at which the interaction force is maximal and the constant-force results would be expected to provide a better description than the constant-velocity ones. Both for this reason and because of the simplification of a power-law description of the final phase of drainage, more attention has been paid here to the constant-force case. The extreme sensitivity of the drainage behavior to any motion in the outer region suggests, however, that more realistic simulations of the actual boundary conditions are desirable. A first attempt to incorporate such conditions in the partially-mobile limit has been made by Abid (1993), using a time-dependent approach velocity derived from equations of motion of the drops during an inertial collision.

Acknowledgements

The authors gratefully acknowledge the financial support of this work by Shell Research and Technology Centre, Amsterdam and by the SON Research Foundation, The Netherlands.

Appendix A. Drainage relations of Yiantsios and Davis, expressed in transformed variables

The first case considered by Yiantsios and Davis concerns the draining film between an immobile deformable drop (radius R) and a plane rigid surface under action of a constant gravitational force,

$$F = \frac{4\pi}{3}\Delta\rho g R^3 \tag{A1}$$

where $\Delta\rho$ is density difference, g acceleration due to gravity, for which they obtain a final drainage rate given by (their equation (37)

$$\frac{h_{\min}}{h_0} = 0.4897\delta\left(\frac{\lambda\Delta\rho g R t}{\mu}\right)^{-1/2}, \tag{A2a}$$

$$\delta = \frac{\Delta\rho g R^3}{\sigma h_0}. \tag{A2b}$$

As observed by Yiantsios and Davis (p. 561, 562), the governing equations in this case are the same as those for drainage between an immobile drop and a plane, immobile deformable interface if δ in Eq. (A2a) is replaced by 2δ:

$$\frac{h_{\min}}{h_0} = 2\times 0.4897\delta\left(\frac{\lambda\Delta\rho g R t}{\mu}\right)^{-1/2}. \tag{A3}$$

From Eq. (2), the equivalent radius for this system is $2R(R_1 = R, R_2 = \infty)$. Eqs. (13) and (A1) now yield $a' = a/2R = (\Delta\rho g R^2/3\sigma)^{1/2}$ and Eq. (A3) may be re-written as

$$h^*_{\min} = \frac{3\times 0.4897}{\sqrt{6}}(\lambda^* t^*)^{-1/2} = 0.5998(\lambda^* t^*)^{-1/2} \tag{A4}$$

which rounds off to give Eq. (32).

When both drop and deformable plane interface are partially mobile, Yiantsios and Davis obtained (their equation (70))

$$\frac{h_{\min}}{h_0} = 0.08\delta\left(\frac{\lambda\Delta\rho g R^{3/2} t}{\mu h_0^{1/2}}\right)^{-2/3} \tag{A5}$$

for a value of δ of 0.025. Making use of the definitions of h^* and t^*, together with Eq. (A2b), Eq. (A5) yields

$$h^*_{\min} = \frac{3 \times 0.08}{2(12\delta)^{1/3}}(t^*)^{-2/3} = 0.1793(t^*)^{-2/3} \tag{A6}$$

which rounds off to give Eq. (31).

References

Abid, S., 1993. Expériences physiques et numériques de coalescence entre deux gouttes immergées dans un autre liquide. PhD thesis, Institut Polytechnique de Toulouse, France.

Abid, S., Chesters, A.K., 1994. The drainage and rupture of partially-mobilr film between colliding drops at constant approach velocity. Int. J. Multiphase Flow 20, 613–629.

Bazhlekov, I.B., van de Vosse, F.N., 1998. Multiple time step approach for numerical simulation of non-Newtonian drop coalescence. In: Iliev, O., Kaschiev, M., Margenov, S., Sendov, Bl., Vassilevski, P. (Eds.), Recent Advances in Numerical Methods and Applications. World Scientific, Singapore, pp. 773–781.

Chesters, A.K., 1991. The modelling of coalescence in fluid–liquid dispersions: a review of current understanding. Trans. Inst. Chem. Engrs. Part A 69, 259–270.

Davis, R.H., Schonberg, J.A., Rallison, J.M., 1989. The lubrication force between two viscous drops. Phys. Fluids A1 (1), 77–81.

Rother, M.A., Zinchenko, A.Z., Davis, R.H., 1997. Buoyancy-driven coalescence of slightly deformable drops. J. Fluid Mech 346, 117–148.

Saboni, A., Gourdon, C., Chesters, A.K., 1995. Drainage and rupture of partially mobile films during coalescence in liquid–liquid systems under a constant interaction force. J. Colloid Interface Sci 175, 27–35.

Yiantsios, S.G., Davis, R.H., 1990. On the buoyancy-driven motion of a drop towards a rigid surface or a deformable interface. J. Fluid Mech 217, 547–573.